*Water* **2014**, *6*, 345-366; doi:10.3390/w6020345

OPEN ACCESS

*water*

**ISSN 2073-4441**

www.mdpi.com/journal/water

*Article*

# Hydrological Flood Simulation Using a Design Hyetograph Created from Extreme Weather Data of a High-Resolution Atmospheric General Circulation Model

**Nobuaki Kimura [1], Akira Tai [2,*], Shen Chiang [1], Hsiao-Ping Wei [1], Yuan-Fong Su [1], Chao-Tzuen Cheng [1] and Akio Kitoh [3]**

[1] National Science and Technology Center for Disaster Reduction (NCDR), Sindian District, New Taipei 231, Taiwan; E-Mails: nkimura3@uwalumni.com (N.K.); johnson@ncdr.nat.gov.tw (S.C.); weihp@ncdr.nat.gov.tw (H.-P.W.); yuanfongsu@ncdr.nat.gov.tw (Y.-F.S.); ctcheng@ncdr.nat.gov.tw (C.-T.C.)

[2] Institute for Advanced Study, Kyushu University, 744 Motooka, Nishi-ku, Fukuoka 8910395, Japan

[3] Faculty of Life and Environmental Sciences, University of Tsukuba, Tsukuba, Ibaraki 3058572, Japan; E-Mail: kito.akio.ff@u.tsukuba.ac.jp

* Author to whom correspondence should be addressed; E-Mail: tai@civil.kyushu-u.ac.jp; Tel.: +81-92-802-3411; Fax: +81-92-802-3411.

*Received: 11 November 2013; in revised form: 24 January 2014 / Accepted: 27 January 2014 / Published: 5 February 2014*

---

**Abstract:** To understand the characteristics of severe floods under global climate change, we created a design hyetograph for a 100-year return period. This incorporates a modified ranking method using the top 10 extreme rainfall events for present, near-future, and far-future periods. The rainfall data sets were projected with a general circulation model with high spatial and temporal resolution and used with a flood model to simulate the higher discharge peaks for the top 10 events of each term in a local watershed. The conventional-like ranking method, in which only a dimensionless shape is considered for the creation of a design hyetograph for a temporal distribution of rainfall, likely results in overestimates of discharge peaks because, even with a lower peak of rainfall intensity and a smaller amount of cumulative rainfall, the distribution shape is the only the factor for the design hyetograph. However, the modified ranking method, which considers amounts of cumulative rainfalls, provides a discharge peak from the design hyetograph less affected by a smaller cumulative rainfall depth for extreme rainfall. Furthermore, the effects of global climate change indicate that future discharge peaks will increase by up to three times of

those of Present-term peaks, which may result in difficult flood control for the downstream river reaches.

**Keywords:** flood; design hyetograph; Tsengwen Reservoir watershed; global climate change

## 1. Introduction

Climate change is likely to have caused numerous occurrences of extreme weather (e.g., severe tropical cyclones and monsoon rainfalls in East Asia) over the last decade and may continue to induce frequent occurrences of extreme weather until the end of the 21st century [1,2]. Owing to extreme weather, severe floods and debris flows have occurred often in Taiwan during the last decade [3]. Floods normally cause serious damage in downstream river regions [4], and therefore it is necessary to gain better information regarding the potential highest peak of discharge, in order both to build and maintain appropriate riverbank defenses and to operate reservoir flood controls. To simulate the highest discharge peak that may occur under global climate change in Taiwan, we focused on two improvements: a detailed data set with higher temporal and spatial resolutions and a better method of representing the artificial temporal distribution of rainfall (a design hyetograph).

When creating the design hyetograph for a return period of a specified number of years, the method used is crucial for high-flow flood simulation. The design hyetograph can be a representative rainfall event that has the fundamental characteristics of an actual storm-induced rainfall event. Normally, in Taiwan a 24-h temporal distribution has been employed with a conventional ranking method [5] with a dimensionless approach [6], which considers the shape of the rainfall distribution. Although there are up-to-date methods, such as the double-triangular method [7] and the stochastic approach [8], which were implemented in a watershed in Taiwan, the ranking method was used in this study because it is a simple and conventional method. The ranking method could be further improved by considering the amount of cumulative rainfall depth as well as the shape of the temporal distribution for an extreme rainfall event. In addition, extending the period of the design hyetograph was considered based on data from recent typhoons [9], which brought large amounts of rainfall beyond the 24-h period.

To achieve a feasible flood simulation, it is important to use a dataset with high resolution, both temporally and spatially, such as that projected by the atmospheric general circulation model (AGCM), which is capable of resolving detailed geographical features. The high-resolution climate change data projected by the AGCM (*i.e.*, 1-h and 20-km intervals) for the entire globe [10–12] covers the East Asia region and is available for the entire island of Taiwan. Although a previous study produced a climate projection for Taiwan downscaled from the output of the AGCMs with relatively coarse resolution [13], high resolution data for future climate change has seldom applied to flood simulation models in Taiwan. In this study, we present a design hyetograph based on the high resolution AGCM data. Our results can provide a good reference for other subtropical and template regions where severe rainstorms may occur.

Our target is to estimate the highest potential peak of river discharge, in a local watershed of Taiwan, as a response to climate change data from a high-resolution AGCM, based on a design hyetograph

created by the modified ranking method, which considers the cumulative-rainfall depths over 24-h or 72-h periods.

## 2. Study Site

The Tsengwen Reservoir watershed is located in southern Taiwan (23°20' N, 120°40' E) and covers parts of Chiayi County, Tainan County, and Kaohsiung County, which is the upper region of the Tsengwen River watershed. The Tsengwen Reservoir watershed is approximately 481 $km^2$. It is surrounded partly by plateau, but primarily by high mountains ranging in height from 233 to 2609 m with a mean slope of approximately 0.54 [14] (Figure 1). There are two rainfall gauge stations within the watershed at locations (120.642° E, 23.423° N) and (120.603° E, 23.336° N) (Figure 1). The watershed impounds a part of the Tsengwen River (138,500-m long) and incorporates the Tsengwen Reservoir, which is the largest in Taiwan and is the major source of water supply for the downstream irrigation system in Chiayi County and Tainan County. The Tsengwen Reservoir has a large net capacity of water storage (approximately 0.5 billion $m^3$), three flood control spillways (9470 $m^3$ $s^{-1}$ maximum capacity) and two outlet channels (150 $m^3$ $s^{-1}$). Mean annual inflow to the reservoir is approximately 1.1 billion $m^3$ [15]. The mean annual air temperature and precipitation are approximately 19 °C and 2700 mm, respectively [14].

**Figure 1.** Map of the Tsengwen Reservoir watershed.

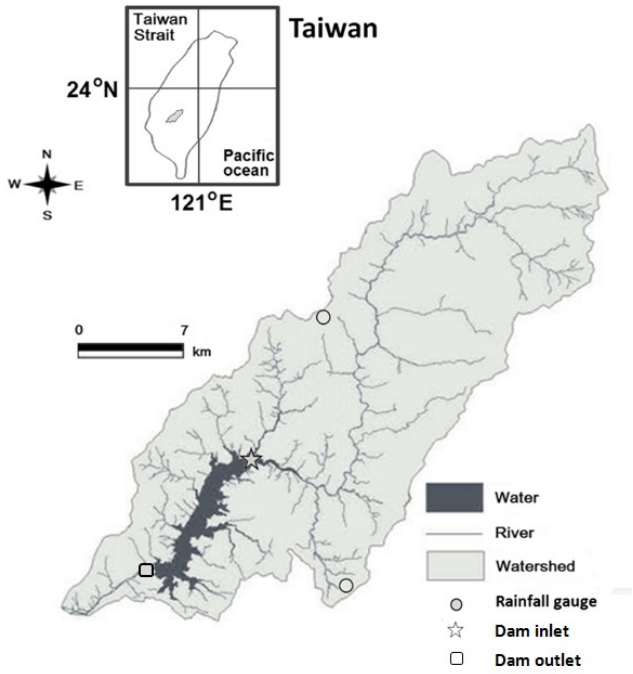


## 3. Method

### *3.1. High Resolution Extreme Weather Data*

In this study, the potential effects of long-term climate change on extreme rainfalls for three terms: Present (1979–2003), Near-future (2015–2039), and Future (2075–2099), were investigated to reveal

the flood characteristics of the peak discharge and cumulative-rainfall depth. Global meteorological data for the three terms were projected by the AGCM of the Japan Meteorological Agency/Meteorological Research Institute (hereafter, MRI-AGCM). In this study, we used the MRI-AGCM3.2S model projected from the MRI-AGCM. The spatial and temporal resolutions of MRI-AGCM3.2S are 20 km horizontally with a 1-h time interval, which is sufficient for investigating the effects of global climate change on tropical cyclones and extreme indices [10–12,16]. As lower boundary conditions for the Present, Near-future, and Future terms, the MRI-AGCM incorporates the observed Sea Surface Temperature (SST) and ensemble SST projected from Phase 3 of the Coupled Model Inter-comparison Project dataset for the A1B scenario of the IPCC, which assumes a global economic and population growth peak in the mid-21st century and then decline [16]. Evaluation of the MRI-AGCM3.2 for the Present term as compared to the observed data has been discussed by Mizuta *et al.* [16]. Endo *et al.* [17] also evaluated the outcomes from the MRI-AGCM against many coupled climate models. The forcing for the future projection in the MRI-AGCM is the same as in Kitoh *et al.* [18]. Here, the data from the MRI-AGCM3.2S with 20-km mesh are called the MRI data.

To downscale the global climate projection to a regional scale, we ran the Weather Research and Forecasting (WRF) model version 3.1.1, driven by the MRI data as the initial and boundary conditions, to simulate a regional climate and to obtain rainfall data with higher spatial and temporal resolutions. No nested-grid treatment and 5-km horizontal resolution cells and 36 vertical layers were implemented in the WRF model in this study. The WRF model employed several appropriate modules and schemes, such as the Community Atmosphere Model, Kain-Fritsch cumulus parameterization, Monin-Obukhov surface layer scheme, Single-Moment 5-class Microphysics scheme, YonSei University boundary scheme, and the Noah land surface module (see [19]). In addition, the spectral nudging method was implemented to enforce the MRI-AGCM variables (*i.e.*, wind velocity, temperature, and geopotential height) above the planetary boundary layer to those of the WRF model by minimizing the climate drift issue.

The rainfall data computed by the WRF model are supposed to capture topographical effects more accurately. The projected rainfall data with hourly intervals were bias-corrected by the statistical method that determines the tuning relations between the projected and observed data through the empirical cumulative distribution function (ECDF). The ECDF of the projected data is close to that of the observed data in descending order [20]. The observed rainfall data were measured at the two rain-gauge stations (Figure 1). For our analysis, the period of the observed data covered approximately 80 typhoon periods from 1979 to 2003 [21]. Here, the dynamical downscaled and biased-corrected data from the MRI data are called the MRI-WRF data.

### *3.2. Artificial Rainfall and Discharge Simulation*

The temporal distribution of extreme rainfall, based on a design hyetograph, was used to estimate the potential higher peak of discharge for a certain return period (100 years in our study) during past or future extreme weather. For the creation of an extreme rainfall distribution, first an extreme rainfall amount for the 100-year return period was computed by frequency analysis of past or future extreme rainfalls during the Present, Near-future, and Future terms (25 years), projected by MRI-WRF data. Then, the temporal distribution of a dimensionless design hyetograph was generated during the three terms. Note that the period of the design hyetograph was set to 24 and 72 h because most past extreme

rainfall events (approximately 51%) persisted beyond 24 h [22]. In particular, Typhoon Morakot (August 2009), which caused severe damages, brought approximately 3 days of continuous heavy rainfall to southern Taiwan. The extreme rainfall distribution was created by multiplying the 100-year-return-period extreme rainfall amount with the dimensionless design hyetograph. Finally, using the extreme rainfall distribution as input data, a flood model simulated the largest potential discharge peak. Those procedures are shown in Figure 2.

**Figure 2.** Process of rainfall creation and discharge simulation. Note that Integrated Flood Analysis System (IFAS) is a flood model.

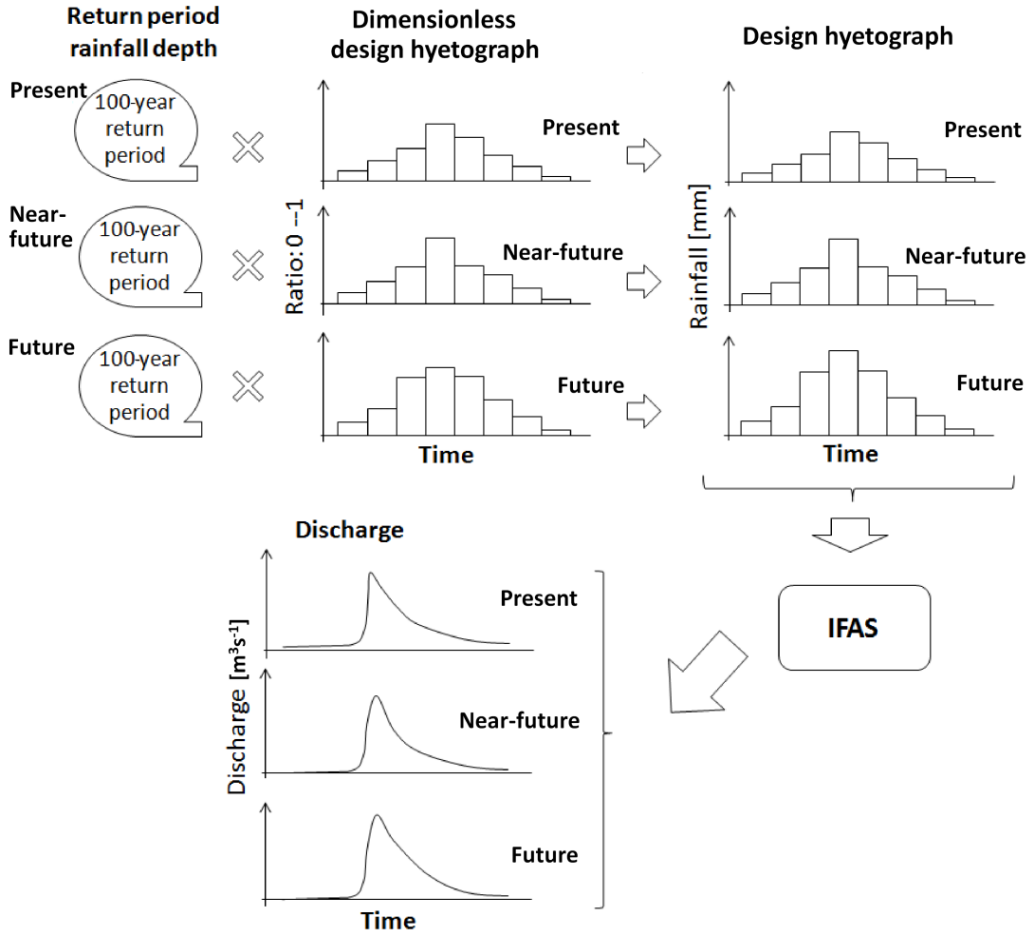


3.2.1. Frequency Analysis

The Log-Pearson Type III (LP3) distribution, proposed by statistician Pearson for a random-variable model [23] and used extensively in hydrologic applications in the United Sates [24] and other countries (e.g., Lu *et al.* [5]), is implemented for the frequency analysis as a probability distribution for fitting the hydrologic data, such as rainfall and discharge data. To estimate the rainfall amount for a target return period with a logarithmic dataset ($X_i$; $i = 1, 2, \ldots, n$), the LP3 distribution requires three parameters: sample mean ($\overline{X}$), standard deviation ($S$) and Skewness coefficient ($C_s$). These parameters are computed respectively, as:

$$\overline{X} = \sum_{i=1}^{n} X_i / n \tag{1}$$

$$S = \sqrt{\sum_{i=1}^{n}\left(X_i - \overline{X}\right)^2 / (n-1)} \tag{2}$$

$$C_S = \frac{n}{S^3(n-1)(n-2)}\sum_{i=1}^{n}\left(X_i - \overline{X}\right)^3 \tag{3}$$

According to Chow *et al.* [25], the logarithm magnitude of a hydrologic event corresponding to each exceedance value is computed by:

$$\log P_T = \overline{X} + K_T S \tag{4}$$

where log $P_T$ is the logarithm of the hydrologic data corresponding to the value of exceedance events and $K_T$ is the frequency factor. The factor $K_T$ employs the approximated equation by Kite [26], given by:

$$K_T = z + \left(z^2 - 1\right)k + \left(z^3 - 6z\right)k^2/3 - \left(z^2 - 1\right)k^3 + zk^4 + k^5/3 \tag{5}$$

where $k = C_S/6$, $C_S$ is the coefficient of skewness of the log-transformed data and $z$ is the standard normal variable, corresponding to an exceedance probability of $1/T$ with $T$ = return period, as defined in:

$$z = W - \frac{2.515517 + 0.802853W + 0.010328W^2}{1 + 1.432788W + 0.189269W^2 + 0.001308W^3} \tag{6}$$

with $W = [\ln(T^2)]^{1/2}$. Note that $P_T$ is rainfall in our study and that the dimensionless equations are applied here.

### 3.2.2. Verification for 100-Year Return Period Data

The 100-year return period was established for the frequency analysis using the rainfall data for 25 years, projected by the MRI-AGCM. A 100-year return period was chosen to satisfy the requirements of flood prevention construction in Taiwan. Although using the 25-year data is possibly insufficient for the frequency analysis of the 100-year return period, we followed the advice from the Taiwan Handbook for Hydrological Design [27], which recommends that the data period should be equal to or more than 25 years for the 100-year return period. Nevertheless, considering the challenges in this type of research, this study could be viewed as a preliminary reference for future climate change. For data verification using frequency analysis, we employed the statistical method of bootstrap resampling [28] to measure uncertainty of the sample estimates in the frequency analysis. The method resamples 99 samples and one original value, corresponding to 100 samples, for the MRI-WRF data of the Present, Near-future, and Future terms. The 24-h and 72-h mean, standard deviation, and 5th and 95th quantiles computed in the method are shown in Table 1. These data are averaged over the Tsengwen Reservoir watershed. The MRI-WRF data for the Present term, adjusted by means of bias correction, involves the properties of the observed data. The indicators (the correlation coefficient and the standard least squares criterion [29]) that evaluate the 24-h goodness-of-fit between the Present MRI-WRF data and the data computed by frequency analysis are approximately 0.98 and 0.04, respectively. These values suggest both data are similar. The 72-h indicators for the goodness-of-fit are very similar to those for 24 h.

**Table 1.** Uncertainty of a 100-year return period depth. Unit is [mm].

| Statistical variable | Present | | Near-future | | Future | |
|---|---|---|---|---|---|---|
| | 24 h | 72 h | 24 h | 72 h | 24 h | 72 h |
| Standard deviation | 125.96 | 252.18 | 192.25 | 242.12 | 327.21 | 667.04 |
| Mean depth | 673.04 | 1312.31 | 1125.34 | 1653.58 | 1884.28 | 3511.55 |
| 5th quantile | 459.15 | 915.17 | 799.06 | 1272.06 | 1342.95 | 2493.82 |
| 95th quantile | 864.43 | 1751.74 | 1434.50 | 2053.11 | 2455.13 | 4669.44 |

3.2.3. Dimensionless Design Hyetograph

A ranking method, based on the mean dimensionless ratio calculated with the hourly rainfall intensities arranged in descending order and the percentages of the total rainfall quantity during 24 h including the peak of rainfall [6], is commonly used in Taiwan to create design hyetographs [5]. Hereafter, this method is called the conventional ranking method. The conventional ranking method takes a percentage of the total quantity for each past extreme rainfall event, arranges the hourly data in descending order as percentages of each rainfall, and then averages over the percentages of these rainfall events at each same ranking position. Finally, the method arranges the mean percentages as a single distribution from the center position (Figure 3a–e). However, being interested in estimates of the largest discharge that may cause severe flood-induced damage during extreme weather, we focused on the generation of a design hyetograph with high intensity, which can represent extreme rainfall events obtained from the MRI-WRF data. Unlike the conventional ranking method, the procedure to calculate the mean among the extreme rainfall events is not performed to avoid losing rainfall characteristics (e.g., temporal distribution shape and period) of individual events, which could potentially create a design hyetograph that may induce the largest discharge peak. This method is called the conventional-like ranking method in this study (Figure 3a–c,d'). In addition, to reduce the effects from a weaker rainfall with a lower rainfall intensity peak or smaller cumulative-rainfall depth among the extreme rainfall events, the ranking method was further modified extensively through consideration of a ranking weighted with cumulative-rainfall depth in descending order (hereinafter, modified ranking method). In contrast to the conventional ranking method, the modified method involves no averaging over the extreme rainfalls; instead, it uses the individual higher-intensity distribution. The modified ranking method was determined from the cumulative-rainfall depths of the projected rainfalls which are the 1st to 10th most extreme events (the top 10 events) by dividing the top 10 cumulative-rainfall depths by the largest cumulative-rainfall depth among the top 10 events (Figure 3f'). Note that the top 10 events were selected by the amount of cumulative rainfall for the entire period of each event in descending order. The modified ranking method coefficient for the top event is defined as 1. The peak of the design hyetograph was placed at the center of the rainfall period, because statistical analysis of the past typhoons (1971 to 1991) revealed that most peaks of typhoon-induced rainfall occur near the center (approximately 43%) in the southern region of Taiwan [22]. The method for generating the temporal distribution of the design hyetograph is to gain the projected rainfall data with hourly time steps for the top 10 events (Figure 3a), take the percentage of the total rainfall quantity for each event, in this study, expressing the hourly-step intensities by a dimensionless ratio (0 to 1) (Figure 3b), arrange the dimensionless hourly ratios in descending order and then pick up the ratios from the largest ratio till the end of the period(e.g., 24 h) for

the design hyetograph (Figure 3c), place the peak value among the ratios at the center position of the distribution (peak at the center), locate the 2nd maximum value at the right side of the center, locate the next maximum ratio at the opposite side of the edge (*i.e.*, the previous maximum position), repeat until the rest of the ratios are empty (Figure 3d') and finally, multiply the ratios with the coefficient of the modified ranking method for each extreme rainfall (Figure 3e'). Note that the initial process (Figures 3a–c) is the same in both ranking methods and the procedures shown in Figure 3a–c,d'–f' were applied to the creation of the 24-h and 72-h design hyetograph. To compare with the modified ranking method, we used the conventional-like ranking method, which is different from the conventional ranking method because of its no-mean approach among the rainfall events (Figure 3d') or is equivalent to the modified ranking method when all the modified ranking method coefficients are one (Figure 3e').

**Figure 3.** Procedure for creating the design hyetograph. Note that the ranking coefficient is the coefficient for the modified ranking method.

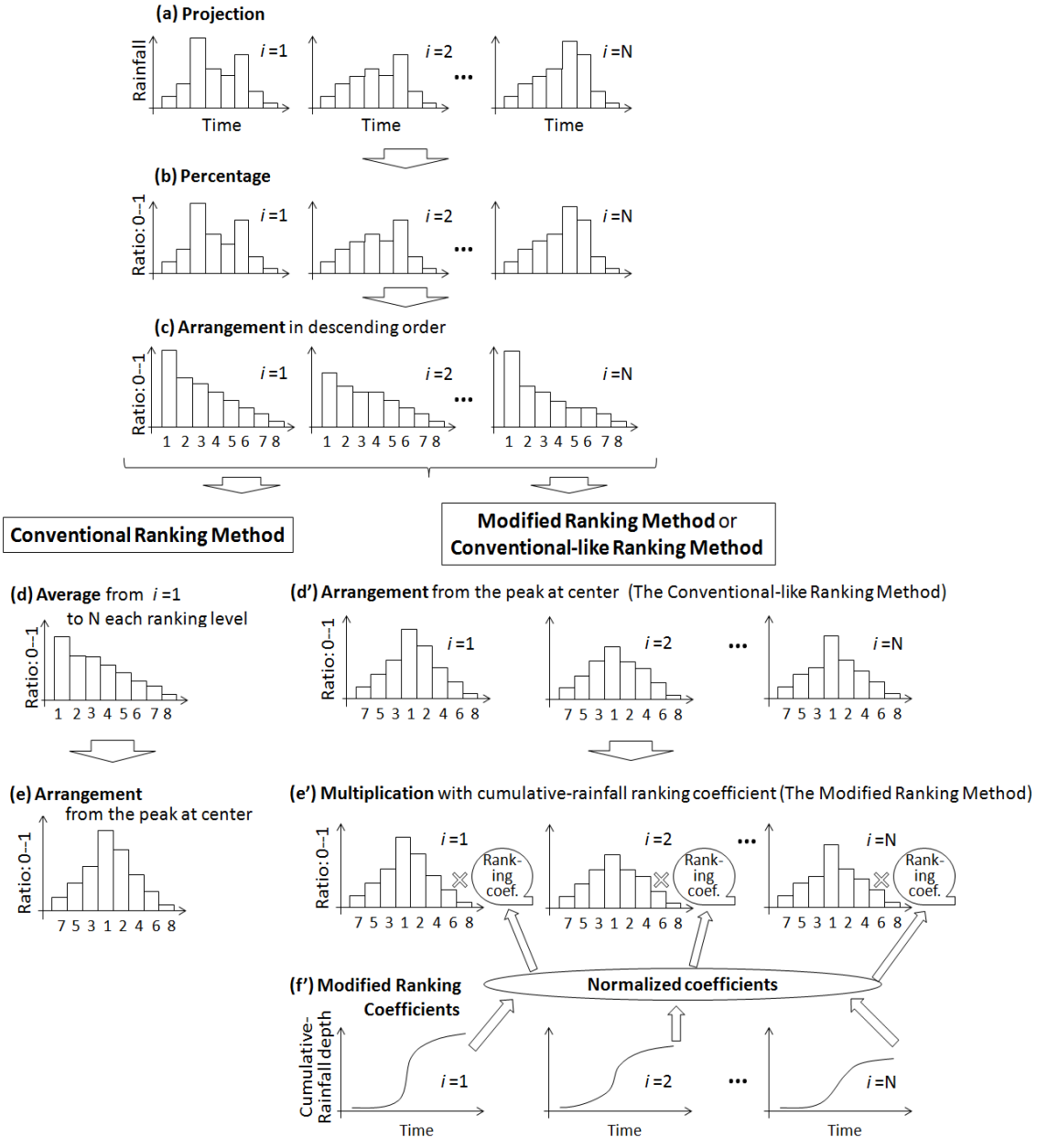

3.2.4. Flood Model

To simulate the larger peak of river discharge caused by extreme rainfall, we used an integrated hydrological simulation system: the Integrated Flood Analysis System (IFAS), which was developed by the International Centre for Water Hazard and Risk Management [30,31]. The IFAS has been applied practically to past flood events in Asian countries, including Japan [31] and Pakistan [32]. A conceptual distributed rainfall-runoff analysis engine, the Public Works Research Institute (PWRI) distributed hydrological model [33], is employed in the IFAS. The PWRI distributed hydrological model divides a target watershed into small cells and computes the flow in each cell through three tanks (surface, groundwater, and river channel tanks) shown in Figure 4. The surface and groundwater tanks were combined as the upper and lower layers in the vertical, respectively, and water evapotranspiration was not applied over the watershed in the present study because the effect of soil moisture on peak discharge is limited. In Taiwan, substantial rainfall is the major factor that affects peak discharge, owing to the short response of discharge to rainfall with the steep terrain [14]. The surface tank simulates the surface flow on the ground, subsurface flow in the upper-layer in the ground, and the percolation to the groundwater tank. The groundwater tank simulates the unconfined groundwater flow from the upper level of the tank and the confined groundwater flow from the lower level of the tank. In the river channel tank, river flow is simulated. A detailed description of the model can be found in Sugiura *et al.* [31] and Aziz and Tanaka [32]. The IFAS has a convenient graphic user interface for the rainfall input of ground-based or satellite-based data and has an input function for GIS-based hydrological features, such as soil and geological types, land-use, climatological zone, and altitude. The numerous coefficients in the distributed hydrological model are set up efficiently through the graphical user interface. The visualization process is also convenient for the user to create the figures and animations related to the hydrological features, possible coupling with a virtual globe map and GIS software (e.g., Google Earth).

**Figure 4.** Schematic diagram of the tank models in the Public Works Research Institute (PWRI)-distributed hydrological model. Note that the flows $Q_{sf}$, $Q_{ri}$, $Q_{g1}$ and $Q_{g2}$ eventually become $Q_{rin}$.

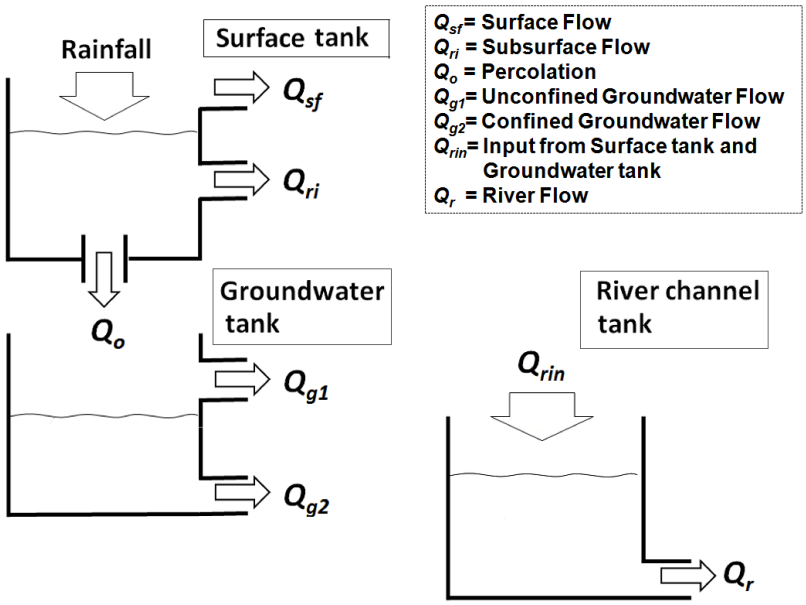

In this study, the IFAS required elevation, land-use, and soil-geology input data. The elevation data were presented by the digital elevation model from altitude information obtained by the shuttle radar topography mission with a 3 arc-second resolution, which is about 90 m (downloaded from HydroSHEDS) [34]. The land-use data with 30 arc-second (≈1 km) resolution were downloaded from Global Map data managed by the International Steering Committee for Global Mapping [35]. The data for the geology and soil type were obtained from the global distribution data for soil water holding capacity with 1° resolution at 0 to 0.3 m from the ground in the United Nations Environment Programme (UNEP) [36]. The projected data (MRI-WRF data) in the Present, Near-future and Future terms at the center of each grid of the WRF model were used for the rainfall input data as ground-based data. The rainfall input data were distributed into several sections of the watershed area using the Thiessen polygon method. This method is a weighted interpolation method that assigns the value of each rainfall input data to the polygon-shaped section, surrounding the point of the input data. The sections are determined by layout of the network stations that record the input data and the construction of perpendicular bisectors to each line between adjacent stations [37]. For the IFAS computational conditions in the Tsengwen Reservoir watershed, the number of cells was 91 × 96 in the horizontal over the entire watershed, *i.e.*, a uniform cell size of 400 m × 400 m. For the determination of all the parameters in the Public Work Research Institute-distributed hydrological model, the default values were employed after manual tuning with a range accepted-value for each parameter. Note that the validation of the PWRI distributed hydrological model in the IFAS for this study site was performed earlier using, appropriate internal parameters associated with geographical and climatological characteristics [38]. It showed 74% reproducibility of the simulated flood discharge and 0.87 for the Nash-Sutcliffe coefficient [39] compared with the observed discharge at the dam inlet for the past typhoon-induced flood event.

### *3.3. Sharpness Evaluation for a Temporal Distribution*

In our study, it is necessary to evaluate the shape of a temporal distribution of rainfall obtained from MRI-WRF data in order to understand how the distribution shape affects the peak of discharge. Generally, Kurtosis (*Kurt*) is introduced to measure the degree of sharpness of a probability distribution. In this study, the $Kurt$ is used as a measure of whether a data profile of rainfall has a flat or sharp peak under the assumption that the profile shape is similar to the shape of the normal distribution with zero mean and unity variance, $N(0,1)$. The *Kurt* is given by:

$$Kurt = \frac{1}{n}\sum_{i=1}^{n}\left(X_i - \overline{X}\right)^4 \Bigg/ \left(\frac{1}{n}\sum_{i=1}^{n}\left(X_i - \overline{X}\right)^2\right)^2 - 3 \tag{7}$$

where a negative $Kurt$ and positive $Kurt$ indicate that the peak is flatter and sharper than that of $N(0,1)$, respectively.

## 4. Results and Discussion

In our study, we are interested only in the most extreme rainfall events selected from 1st to 10th place (hereinafter TP 1 to TP 10) during each term (Present, Near-future or Future). The TP 1 to TP 10 (top 10 events) were defined by ranking the cumulative-rainfall depths for the entire period. These rainfall events in each term were represented by artificial rainfall distributions (*i.e.*, design hyetographs)

computed by the 100-year-return-period rainfall amounts and the dimensionless ratios provided by the conventional and modified-ranking methods for 24- or 72-h periods.

### *4.1. Use of Design Hyetograph without Modified Ranking Method Coefficients*

The dimensionless design hyetographs for TP 1 to TP 10 were created based upon the conventional ranking method without mean distribution among the top 10 rainfall events and without the modified ranking method coefficients. This conventional-like ranking method differs from the conventional method in that it does not calculate the mean. Figure 5 shows the temporal distribution of the dimensionless design hyetographs, generated by the conventional-like ranking method, and the normalized cumulative-rainfall depths for 24-h and 72-h periods from TP 1 to TP 10. Higher peak intensities (steeper shapes) of the distributions for both periods appear even for those extreme rainfalls with lower positions (e.g., TP 7 and TP 10). It is natural that these higher peaks appeared because only the distribution shape was considered in the generation of the dimensionless design hyetographs. In particular, the cumulative rainfall depths at the higher places (e.g., TP 1 to TP 3) for the 24-h period are likely to linearly increase compared with those for the 72-h period because the selected 24 intensities are likely to be similar.

**Figure 5.** Present-term temporal distribution of normalized rainfall, averaged over the upper stream area from the dam inlet, from TP 1 to TP 10 for (**a**) 24-h; and (**b**) 72-h periods without the modified ranking method coefficients.

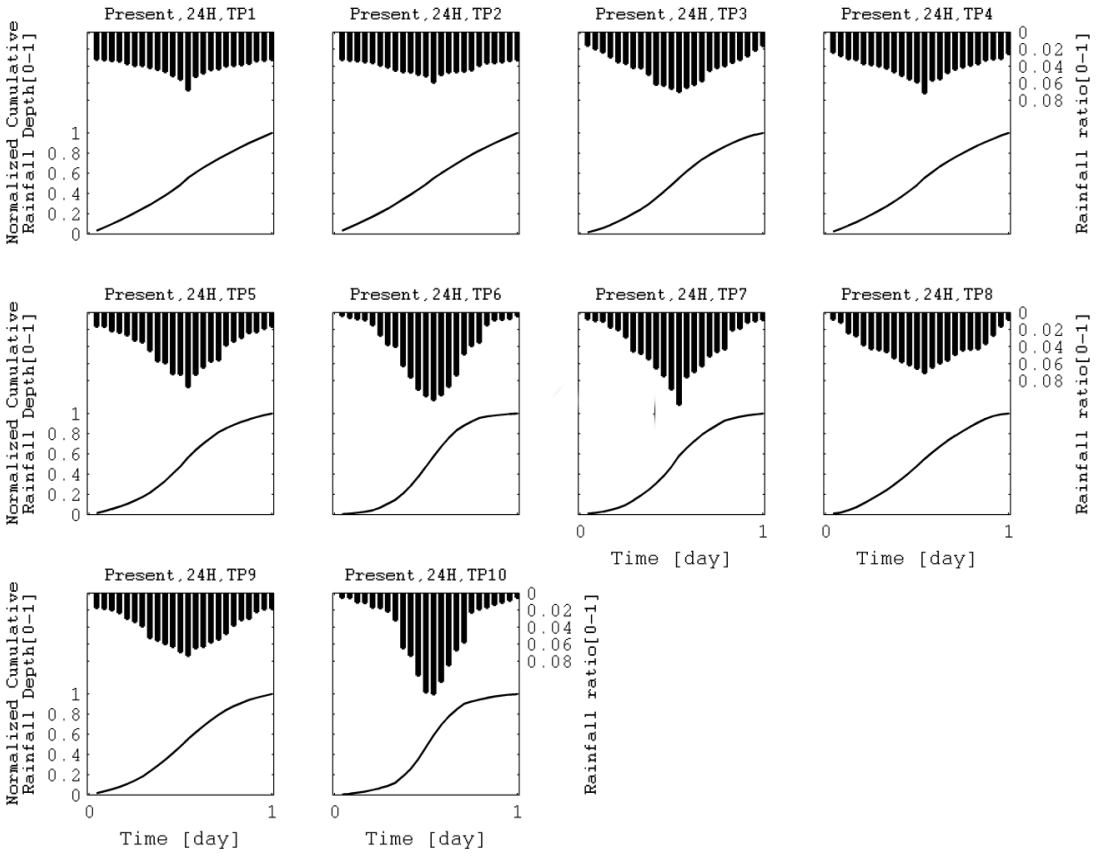


(**a**)

**Figure 5.** *Cont.*

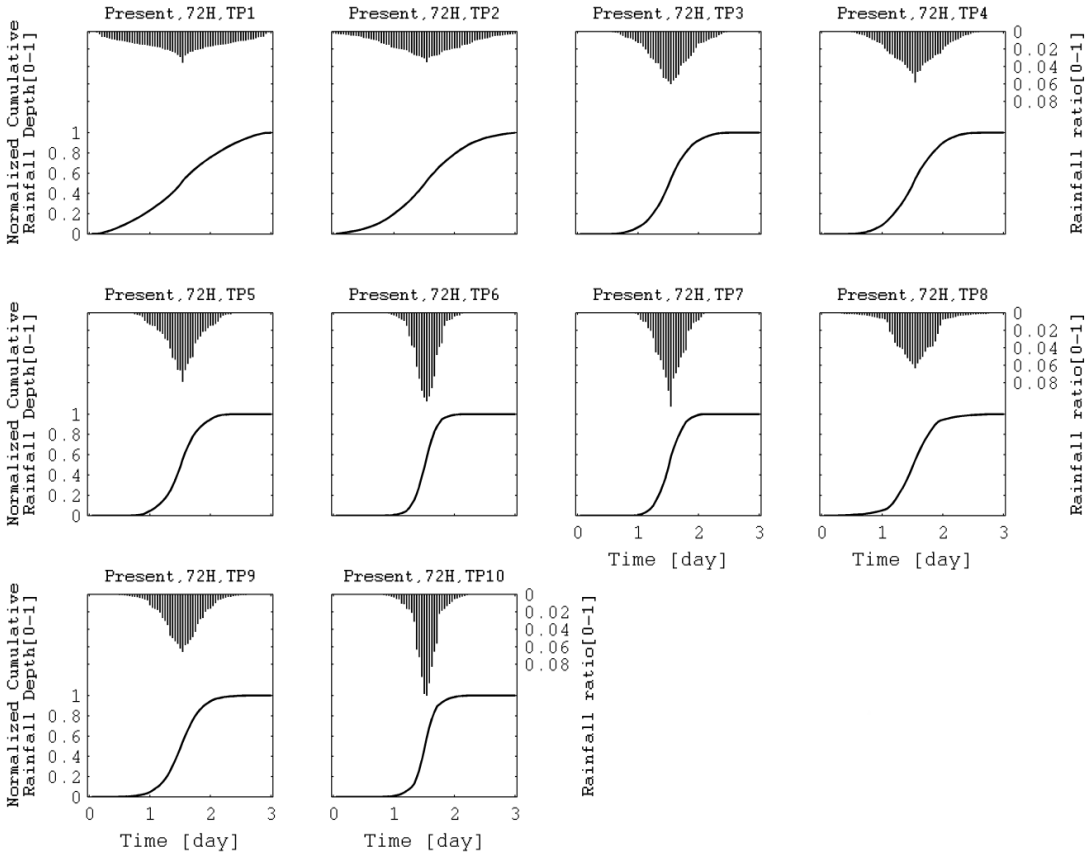


(**b**)

Using the design hyetographs computed by the dimensionless hyetographs and the 100-year-return-period rainfall amounts, the temporal distributions of discharge were simulated using the IFAS from TP 1 to TP 10. The distributions of discharge and design hyetograph at the dam inlet from TP 1 to TP 3 for each period (24 or 72 h) in the Present term are shown in Figure 6. Note that the dam inlet chosen for the comparison among the top 10 discharge peaks is able to eliminate the influence of spillway-based flood control operations at the outlet of the dam on the discharge peaks. For TP 1, both peaks of discharge for the 24- and 72-h periods are similar with only 2% difference, which is likely less affected by cumulative-rainfall depth and sharpness differences (Table 2). However, the peak for 72-h period (approximately 3503 $m^3 s^{-1}$) is 10% higher than that for the 24-h period for the TP 2 event (Figure 5b,e). If the cumulative-rainfall depth for the 24-h period is defined as 1, the rate of cumulative-rainfall depth for the 72-h period to the 24-h cumulative-rainfall depth is approximately 1.9. This peak of discharge is likely affected by the difference of cumulative-rainfall depths, dependent upon the period length. The *Kurt* for the rainfall distributions for the two periods (24 and 72 h) is −1.00 and −0.28, respectively (see Present-TP1 in Table 2), which indicates the 72-h distribution is sharper than the 24-h distribution. Furthermore, for TP 3 (Figures 5c and f), the longer period has a higher peak of discharge because the cumulative-rainfall depth for 72 h was increased by 1.9 times compared with the 24-h cumulative-rainfall depth and the sharpness for 72 h was increased by approximately 28% compared with the 24-h sharpness (Present-TP3 in Table 2). These results suggest that the height of the discharge peak can be determined by not only the sharpness of the rainfall distribution, but also by the

cumulative-rainfall depth. Figure 7 shows the peaks of discharge for TP 1 to TP 10 for the two periods (24 and 72 h) during the Present term. Although the TP 1 and TP 2 cases were simulated with the design hyetographs from the top two extreme rainfalls, the peaks of TP 1 and TP 2 are smaller than the other peaks (below TP 3), whose volumes of discharge should be lower than those of TP 1 or TP 2. In addition, the peaks of discharge for TP 10 for 24 and 72 h are the highest among all the cases; this is likely caused by the sharpness of the design hyetograph distribution. In fact, the sharpness values of the TP 10 design hyetograph for 24 and 72 h are 0.52 and 1.18, respectively, which are the highest value among the top 10 design hyetographs for each period. This implies that a sharper distribution of the design hyetograph produces a higher peak of discharge, even with the same rainfall amount, computed by a 100-year return period in the Present term. Note that the cumulative-rainfall depths for 24 and 72 h are approximately the same from TP 1 to TP 10, because the return period rainfall amounts for these periods are the same and it is only the distribution shapes of their design hyetographs that are different.

**Figure 6.** TP 1 to TP 3 rainfalls and discharges, (**a**,**b**,**c**) for 24-h and (**d**,**e**,**f**) for 72-h periods without the modified ranking method coefficients. Note that the rainfalls were averaged over the upper stream area from the dam inlet and cms is the unit of [$m^3$ $s^{-1}$] in the figure boxes.

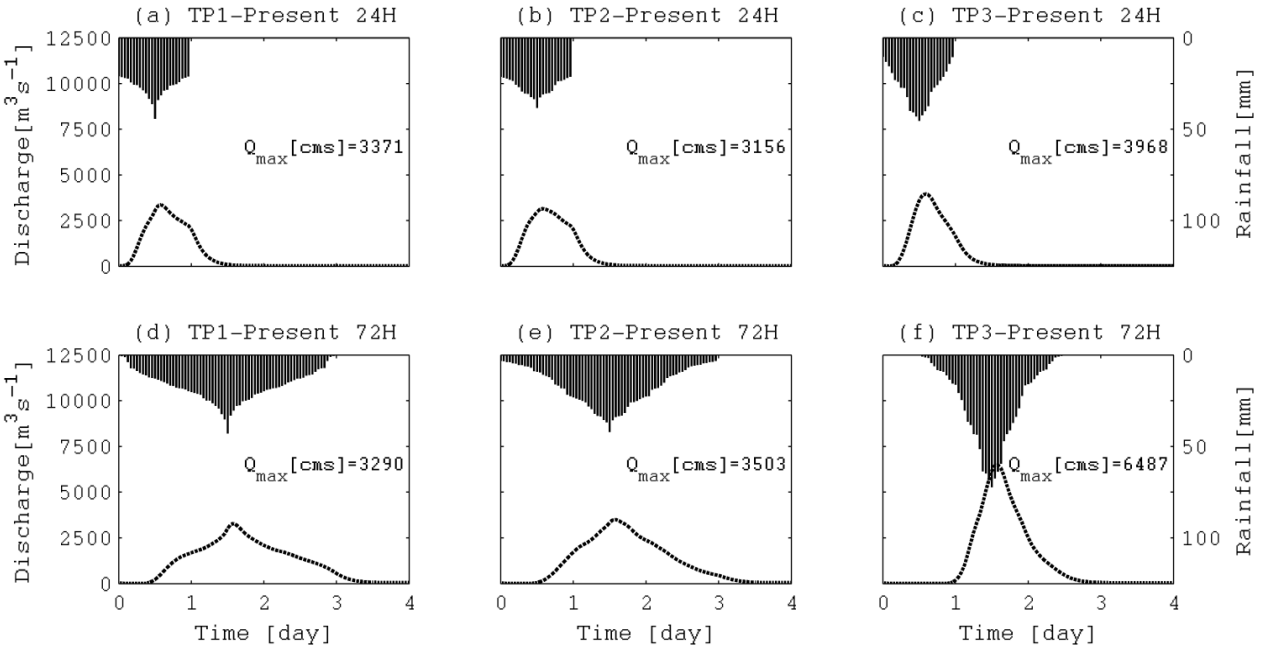


*4.2. Use of Design Hyetograph with the Modified Ranking Method Coefficients*

To reduce excessive effects from weaker extreme rainfalls due to consideration only of the sharpness of the design hyetographs (the steep "mountain-type" distributions in the dimensionless expression), as seen in Figure 7, normalized modified ranking method coefficients were introduced for both periods. The normalized modified ranking method coefficients were computed by the cumulative-rainfall depths corresponding to the top 10 extreme rainfalls, divided by the largest cumulative-rainfall depth. The dimensionless design hyetographs of the modified ranking method were created by the multiplication of the modified ranking method coefficients in descending order from TP 1 to TP 10 as in Figure 3e'. The dimensionless design hyetographs and the normalized

cumulative rainfall depths from TP 1 to TP 10 for 24-h and 72-h periods are shown in Figure 8. Because the modified ranking method coefficients for the top 10 events are in descending order, the dimensionless distributions for the design hyetograph and the normalized cumulative-rainfall depths are decreased for both the 24-h and 72-h periods. The peak intensities for the stronger extreme rainfalls, such as TP 1, TP 2 and TP 3 are higher than those of the weaker rainfalls (e.g., TP 9 and TP10), which indicate that the modified temporal distributions become feasible depending upon the strength of their rainfall intensities. Figure 9a shows the peaks of discharge from TP 1 to TP 10 for the two periods during the Present term under the consideration of the modified ranking method coefficients. The peak of discharge for the 72-h period is a higher than that for the 24-h peak at each extreme event because the 72-h cumulative-rainfall depth is larger. The TP 3 peaks are the highest among the peaks of the other events, even greater than TP 1 and TP 2 peaks with larger cumulative-rainfall depths, because the temporal distributions of the TP 3 design hyetograph are sharper than for TP 1 and TP 2. In fact, through the quantitative evaluation of sharpness ( *Kurt* ), the *Kurt* for TP 3 during the 24-h period is higher than that for both TP 1 and TP 2 by 37% and 41%, respectively (Table 3). For the *Kurt* during the 72-h period, the comparison between TP 3 and TP 1 or TP 2 is similar to the result for the 24-h. Figure 9a also shows that the peaks below TP 4 become lower than TP 1 to TP 3 as the design hyetographs were modified by the modified ranking method coefficients. Note that the cumulative-rainfall depth for TP 2 in the 24-h period was larger than that for TP 1 with an approximately 8% increase (Table 3). This is because the ranking for the top 10 extreme rainfall events was determined by the cumulative-rainfall depths for the entire period, which were mostly over 72 h. Therefore, the descending order for the cumulative-rainfall depths for 24 h was slightly different from that for the top 10 events, but the order for 72 h was consistent with that for the top 10 events.

**Table 2.** Cumulative-rainfall depth and Kurtosis (*Kurt*) for the design hyetograph without the modified ranking method coefficients for the Present term. Note that the values associated with the design hyetograph were averaged over the upper stream area from the dam inlet and that slightly different rainfall depths among the top 10 events were caused by computational errors (maximum 0.05% for 24 h and 0.30% for 72 h against mean depths) from frequency analysis.

| Top 10 events | 24 h | | 72 h | |
|---|---|---|---|---|
| | **Cumulative-rainfall depth (mm)** | **Kurtosis (none-unit)** | **Cumulative-rainfall depth (mm)** | **Kurtosis (none-unit)** |
| Present-TP 1 | 648.0 | −0.97 | 1202.1 | −0.70 |
| TP 2 | 648.2 | −1.00 | 1203.6 | −0.28 |
| TP 3 | 648.2 | −0.72 | 1202.3 | −0.03 |
| TP 4 | 648.0 | −0.88 | 1202.1 | −0.24 |
| TP 5 | 648.0 | −0.46 | 1201.8 | −0.01 |
| TP 6 | 648.3 | 0.06 | 1200.3 | 0.40 |
| TP 7 | 648.2 | −0.24 | 1201.8 | −0.14 |
| TP 8 | 648.3 | −0.81 | 1201.5 | 1.40 |
| TP 9 | 648.2 | −0.61 | 1199.8 | 0.35 |
| TP 10 | 648.1 | 0.52 | 1201.1 | 1.18 |

**Figure 7.** Present-term peaks of discharge from TP 1 to TP 10 without the modified ranking method coefficients for each period (24 and 72 h) at the dam inlet.

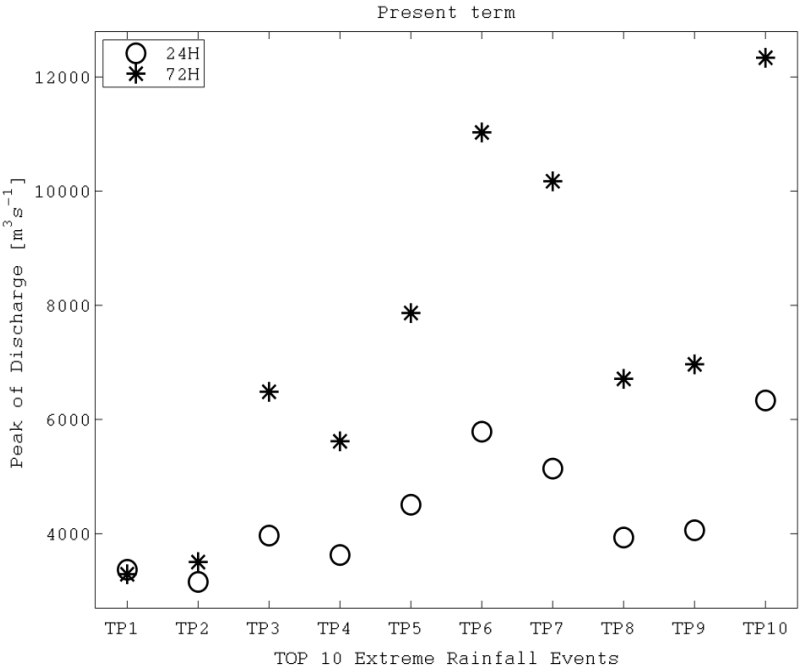


**Figure 8.** Present-term temporal distribution of normalized rainfall, averaged over the upper stream area from the dam inlet, from TP 1 to TP 10 for (**a**) 24-h; and (**b**) 72-h periods with the modified ranking method coefficients.

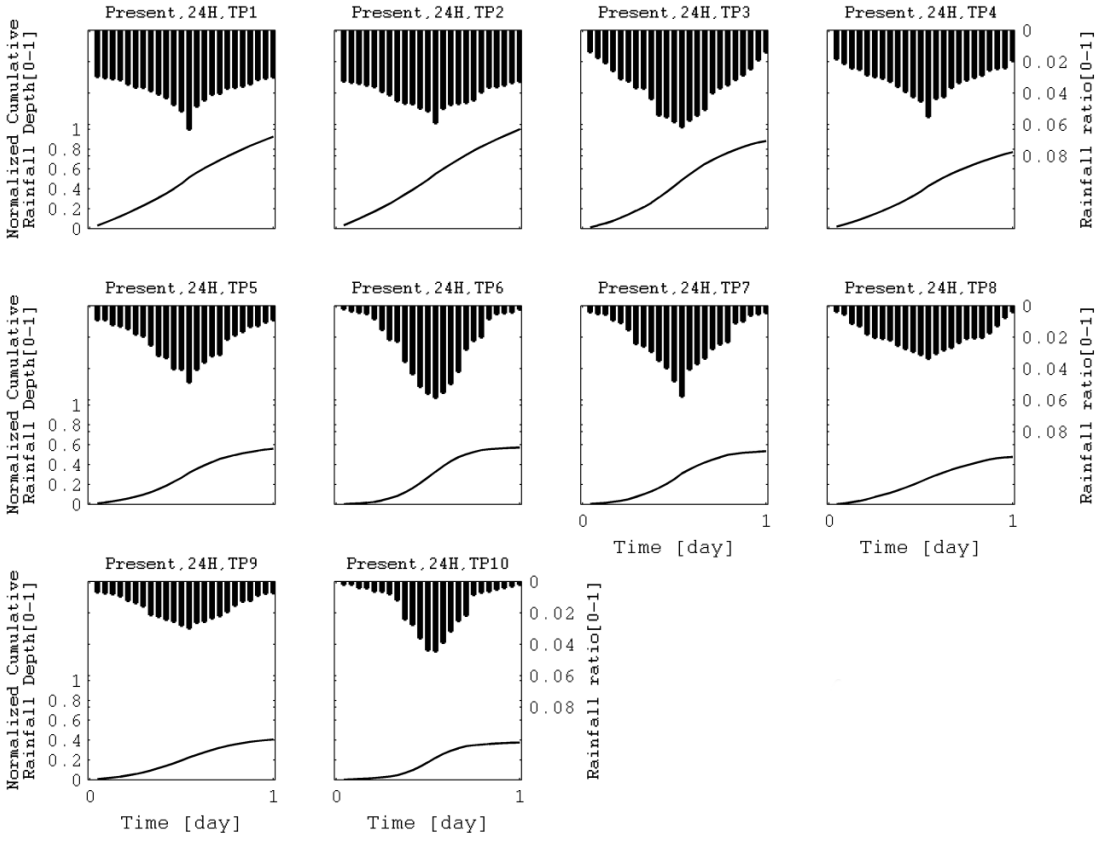


**(a)**

**Figure 8.** *Cont.*

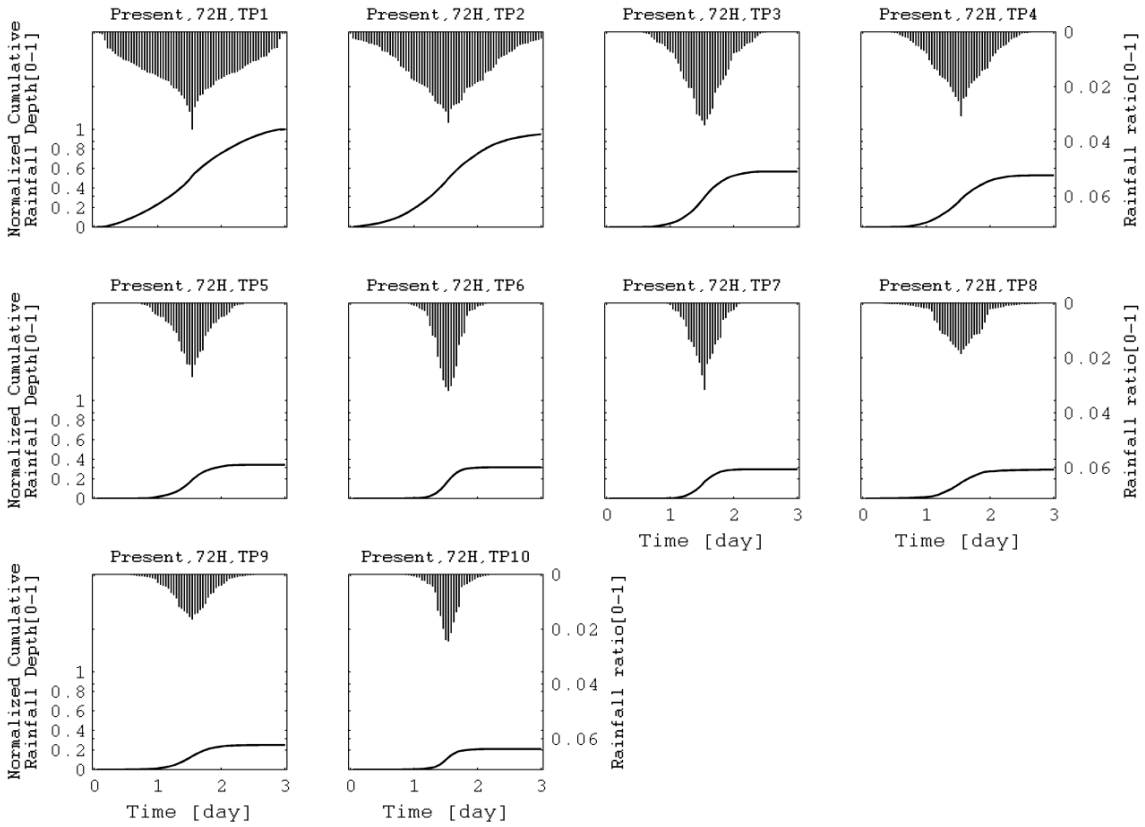


(**b**)

**Figure 9.** Peaks of discharge from TP 1 to TP 10 with the modified ranking method coefficients for each period (24 and 72 h) at the dam inlet for (**a**) Present; (**b**) Near-future; and (**c**) Future terms.

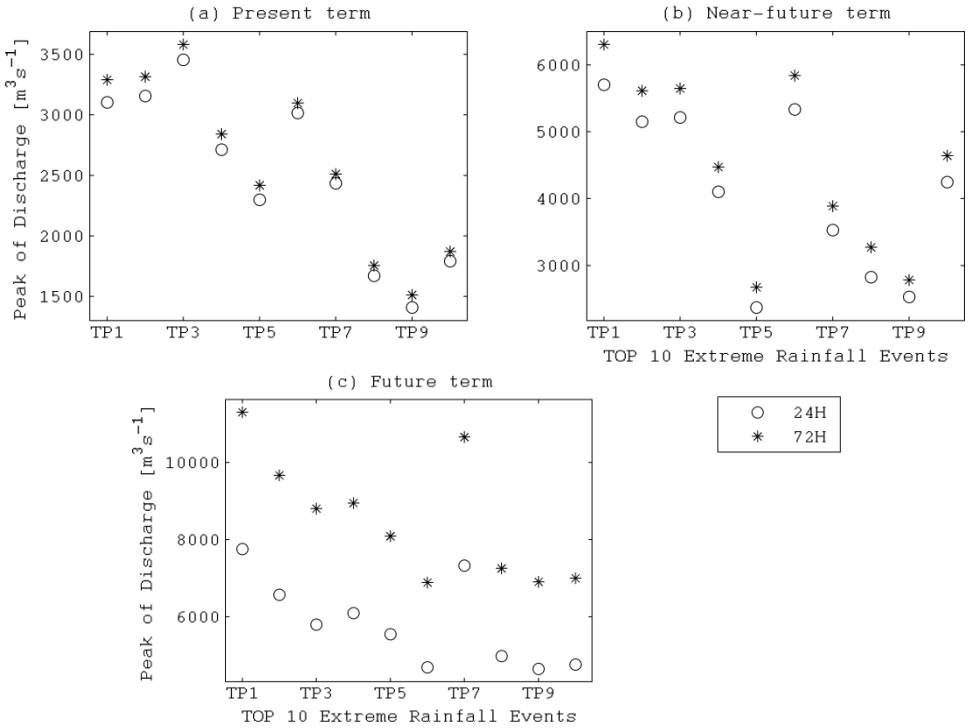

**Table 3.** Cumulative-rainfall depth and Kurtosis (*Kurt*) for design hyetograph with the modified ranking method coefficients for the Present, Near-future, and Future terms. Note that the values associated with the design hyetograph were averaged over the upper stream area from the dam inlet.

| Top 10 events | 24 h | | 72 h | |
|---|---|---|---|---|
| | Cumulative-rainfall depth (mm) | Kurtosis (none-unit) | Cumulative-rainfall depth (mm) | Kurtosis (none-unit) |
| Present-TP 1 | 595.5 | −0.97 | 1256.1 | −0.70 |
| TP 2 | 642.7 | −1.00 | 1193.6 | −0.28 |
| TP 3 | 566.7 | −0.71 | 713.1 | −0.05 |
| TP 4 | 495.1 | −0.87 | 662.5 | −0.24 |
| TP 5 | 359.7 | −0.46 | 430.7 | −0.02 |
| TP 6 | 367.2 | 0.05 | 397.2 | 0.40 |
| TP 7 | 343.8 | −0.24 | 371.7 | −0.14 |
| TP 8 | 305.9 | −0.81 | 367.4 | 1.41 |
| TP 9 | 261.2 | −0.60 | 315.2 | 0.53 |
| TP 10 | 241.4 | 0.52 | 264.5 | 1.15 |
| Near-future-TP 1 | 959.9 | −0.84 | 1424.1 | −0.20 |
| TP 2 | 974.1 | −0.91 | 1142.3 | −0.78 |
| TP 3 | 956.7 | −0.96 | 1099.7 | −0.70 |
| TP 4 | 783.4 | −0.94 | 915.6 | −0.75 |
| TP 5 | 485.8 | −0.99 | 898.3 | −0.41 |
| TP 6 | 709.7 | −0.43 | 818.4 | 0.48 |
| TP 7 | 610.0 | −0.85 | 759.4 | −0.34 |
| TP 8 | 414.6 | −0.46 | 656.7 | 0.54 |
| TP 9 | 446.0 | −0.71 | 529.0 | −0.01 |
| TP 10 | 466.1 | −0.27 | 497.7 | −0.27 |
| Future-TP 1 | 1466.5 | −0.98 | 2675.4 | −0.68 |
| TP 2 | 1205.1 | −0.90 | 2459.0 | −0.52 |
| TP 3 | 977.0 | −0.92 | 2186.1 | −0.28 |
| TP 4 | 1225.5 | −1.02 | 2083.8 | −0.57 |
| TP 5 | 1116.4 | −1.03 | 1870.6 | −0.45 |
| TP 6 | 862.6 | −0.85 | 1789.1 | −0.49 |
| TP 7 | 1042.4 | −0.74 | 1474.7 | −0.73 |
| TP 8 | 844.5 | −0.81 | 1271.1 | −0.73 |
| TP 9 | 732.7 | −0.75 | 1232.8 | 0.21 |
| TP 10 | 736.3 | −0.60 | 1235.9 | −0.10 |

Under the impact of future climate change, the design hyetographs of the top 10 events for each term of the Near-future and Future were created for 24-h and 72-h periods using the modified raking method. For the Near-future, the cumulative rainfall depths from the design hyetographs were 1.4–1.9 times larger than for the 24-h period, and were 1.0–2.1 times equivalent and larger than for the 72-h period of the Present term. For the Future terms, the cumulative rainfall depths were 1.7–3.1 and 2.1–4.7 times larger than for the 24-h and 72-h periods of the Present term, respectively (Table 3). In addition, the peaks of the 24-h design hyetographs of the top 10 events for the Present term ranged from 19.1 to 40.6 mm.

The 24-h peaks for the Near-future and Future terms increased by up to 2.4 and 2.9 times for the Present term, respectively. The Near-future and Future 72-h peaks were also larger than for the Present term by up to 2.4 and 3.9 times, respectively. These data suggest that the projected future extreme rainfall events will be more severe than those of for the Present term. The peaks of the discharge for the two periods for the Near-future term with the modified ranking method coefficients are shown in Figure 9b. The discharge peaks of the 72-h period for each extreme rainfall event (TP 1 to TP 10) are higher than the 24-h period because the 72-h cumulative-rainfall depth and sharpness are larger. The discharge peaks of TP 1 for 24 and 72 h are the highest among those of the other events. This result implies that the modified ranking method coefficients affect those peaks directly. However, the peaks for TP 3, TP 6 and TP 10 are relatively higher than those positioned in front. These results suggest that it is likely the distribution sharpness of the design hyetograph affects the peak of discharge. Furthermore, the peak of TP 5 for the 24-h period is much lower than those positioned behind, which could be affected by both cumulative-rainfall depth and sharpness. Figure 9c shows the peaks of discharge among the top 10 events of the Future term. The peak heights are dependent upon the period of each event primarily because of an amount of cumulative rainfall. In Particular, the peaks of TP 7 are relatively higher, except they are approximately equivalent to the TP 1 peaks. This is likely because of both the strong sharpness of the distribution and the large cumulative-rainfall depth for TP 7's 24-h design hyetograph; however, the distributions of TP 7's 72-h design hyetograph do not have higher *Kurt* than those positioned in front (TP 5 and TP 6). The reason for this is that the TP 7 distribution had strong sharpness around the peak (only within 3 to 4 h) with 30% increase, which suggests that Kurtosis cannot evaluate appropriately this kind of sharpness because of the assumption that the distribution shape should be similar to that of $N(0,1)$.

As our study site contains the large reservoir in Taiwan (Tsengwen Reservoir), the discussion of future flood risk management under future climate change is meaningful through the higher peak of discharge for the top 10 events. The maximum peaks for all terms are approximately 3600 $m^3 s^{-1}$ for TP 3, 72-h period in the Present term, approximately 6300 $m^3 s^{-1}$ for TP 1, 72-h period in the Near-future term, and approximately 11,300 $m^3 s^{-1}$ for TP 1, 72-h period in the Future term (Figures 9), *i.e.*, the peaks of discharge for the Near-future and Future terms are increased by 1.7 and 3.1 times that of the peak for the Present term, respectively. If an extreme rainfall event with a longer period were to occur, those maximum peaks of discharge could be generated, which may result in problems of flood control at the dam outlet of the Tsengwen Reservoir. The upstream watershed area for the discharge peaks simulated at the dam inlet was different from that at the dam outlet, because of the approximately 30% extended area from which the rainfall flowed directly to the reservoir. Therefore, the simulated peak discharge data were obtained from the dam outlet. The peaks of the discharge at the dam outlet for the 72-h, TP 1, the Near-future and Future terms were 7792 $m^3 s^{-1}$ and 13,881 $m^3 s^{-1}$, respectively. In fact, the maximum peak of discharge for the 72-h TP 1 in the Future term is above the maximum capacity of the dam spillway (9620 $m^3 s^{-1}$). In addition, the design peak of the discharge for a 100-year return period at Yufong Bridge on the downstream river reaches (about 10 km from the dam) is 6900 $m^3 s^{-1}$ [40]. Therefore, in order to prevent the worst extreme event possible, the dam spillway capacity should be limited to less than 6900 $m^3 s^{-1}$. Even if the spillway capacity can handle successfully the reduced highest peak, the excess water must remain in the reservoir. The estimates for the excessive water for the Near-future and Future terms was 0.01 billion $m^3 s^{-1}$ and 0.31 billion $m^3 s^{-1}$, corresponding to

approximately 2% and 62% of the total reservoir capacity, respectively. However, those percentages are likely optimistic because we have ignored the effects of sediment and driftwoods on reservoir capacity [41] and the extensive watershed that exists between the dam outlet and the Yufong Bridge. The estimated excess water for the Future term suggests that dam flood control might have potential risks.

In this study, discharge simulations were conducted using only MRI-WRF data from the MRI-AGCM3.2S; however, there are many outcomes possible from using different types of global AGCM or from using the MRI-AGCM implemented with different types of initial and boundary conditions (e.g., Endo *et al.* [17]). Using these results, an uncertainty analysis can be conducted with the IFAS to understand the uncertainty characteristics, which may suggest the accuracy of the input/output data for the IFAS. Therefore, as future work, it is necessary to evaluate the uncertainty trend with statistical analysis for different kind of inputs and outputs in the IFAS simulation.

## 5. Conclusions

Using the design hyetographs, which were created using the ranking method for two periods (24 and 72 h) and 100-year return-period rainfall amounts provided by the high-resolution spatial and temporal MRI-WRF data with dynamic downscaling and bias-correction during long-term climate change (*i.e.*, three terms: Present, Near-future, and Future), the IFAS simulated the peaks of discharge for extreme rainfall events (TP 1 to TP 10) in each term. When the design hyetographs were generated by the conventional-like ranking method with the dimensionless approach, the peaks of discharge simulated by the IFAS were overestimated for weaker extreme rainfall with lower peaks or smaller cumulative-rainfall depths, because only the sharpness of the dimensionless rainfall distribution was taken into account. To improve this problem of overestimation, the modified ranking method coefficients in descending order were introduced when the design hyetographs were created. With the modified ranking method coefficients, feasible peaks of discharge were obtained with the assumption that a design hyetograph with a larger cumulative rainfall depth normally provides a higher peak of discharge. The peaks of discharge under future climate change become higher than the peaks for the Present term. In Particular, the highest peak of discharge for the Future term implies that there is a potential risk for flood control based on the design peak of discharge with 100-year return period for the downstream river reaches in the study area.

## Acknowledgments

We are grateful for the use of the IFAS package from Fukami Kazuhiko of the International Centre for Water Hazard and Risk Management. We extend our deep appreciate the financial support by the Taiwan National Science Council (NSC 100-2621-M-492-001). This work is also supported by the SOUSEI Program of the Ministry of Education, Culture, Sports, Science and Technology of Japan.

## Conflicts of Interest

The authors declare no conflict of interest.

## References


1. Intergovernmental Panel on Climate Change (IPCC). *Fourth Assessment Report of the IPCC*; Solomon, S., Qin, D., Manning, M., Chen, Z., Marquis, M., Averyt, K.B., Tignor, M., Miller, H.L., Eds.; Cambridge University Press: Cambridge, UK; New York, NY, USA, 2007; p. 996.
2. Intergovernmental Panel on Climate Change (IPCC). *Managing the Risks of Extreme Events and Disasters to Advance Climate Change Adaptation*; A Special Report of Working Groups I and II of the Intergovernmental Panel on Climate Change; Field, C.B., Barros, V., Stocker, T.F., Qin, D., Dokken, D.J., Ebi, K.L., Mastrandrea, M.D., Mach, K.J., Plattner, G.-K., Allen, S.K., *et al*, Eds.; Cambridge University Press: Cambridge, UK; New York, NY, USA, 2012; p. 582.
3. Ge, X.; Li, T.; Zhang, S.; Peng, M. What causes the extremely heavy rainfall in Taiwan during Typhoon Morakot 2009? *Atmos. Sci. Lett*. **2010**, *11*, 46–50.
4. Chu, H.J.; Pan, T.Y.; Liou, J.J. Extreme precipitation estimation with typhoon Morakot using frequency and spatial analysis. *Terr. Atmos. Ocean. Sci*. **2011**, *22*, 549–558.
5. Lu, H.S.; Hwang, L.S.; Lin, J.P.; Lin, C.L.; Wang, C.H. Design hyetograph estimation of different durations in the Fushan area of north-eastern Taiwan (in Chinese). *J. Chin. Soil Water Conserv*. **2007**, *38*, 399–415.
6. Huff, F.A. Time distribution of rainfall in heavy storms. *Water Resour. Res*. **1967**, *3*, 1007–1019.
7. Lee, K.T.; Ho, J.Y. Design hyetograph for typhoon rainstorms in Taiwan. *J. Hydrol. Eng*. **2008**, *13*, 647–651.
8. Lin, G.F.; Chen, L.H.; Kao, S.C. Development of regional design hyetographs. *Hydrol. Process*. **2005**, *19*, 937–946.
9. Chien, F.C.; Kuo, H.C. On the extreme rainfall of Typhoon Morakot (2009). *J. Geophys. Res*. **2011**, *116*, doi:10.1029/2010JD015092.
10. Oouchi, K.; Yoshimura, J.; Yoshimura, H.; Mizuta, R.; Kusunoki, S.; Noda, A. Tropical cyclone climatology in a global-warming climate as simulated in a 20 km-mesh global atmospheric model: Frequency and wind intensity analyses. *J. Meteorol. Soc. Japan* **2006**, *84*, 259–276.
11. Mizuta, R.; Oouchi, K.; Yoshimura, H.; Noda, A.; Katayama, K.; Yukimoto, S.; Hosaka, M.; Kusunoki, S.; Kawai, H.; Nakawaga, M. 20-km-mesh global climate simulations using JMA-GSM model. *J. Meteorol. Soc. Japan* **2006**, *84*, 165–185.
12. Kitoh, A.; Yatagai. A.; Alpert, P. First super-high-resolution model projection that the ancient "Fertile Crescent" will disappear in this century. *Hydrol. Res. Lett*. **2008**, *2*, 1–4.
13. Liu, C.M.; Wu, M.C.; Paul, S.; Chen, C.Y.; Lin, S.H.; Lin, W.S.; Lee, Y.C.; Hsu, H.H.; Tzeng, R.Y.; Chen, C.T. Super-ensemble of three RCMs for climate projection over East Asia and Taiwan. *Theor. Appl. Climatol*. **2011**, *103*, 265–278.
14. Tung, C.P. Climate change impacts on water resources of the Tsengwen creek watershed in Taiwan. *J. Am. Water Resour. As*. **2001**, *37*, 167–176.
15. Taiwan Water Resources Agency (WRA). *Hydrological Year Book of Taiwan* (in Chinese); Republic of China Ministry of Economic Affairs: Taipei, Taiwan, 2004.

16. Mizuta, R.; Yoshimura, H.; Murakami, H.; Matsueda, M.; Endo, H.; Ose, T.; Kamiguchi, K.; Hosaka, M.; Sugi, M.; Yukimoto, S.; *et al*. Climate simulations using MRI-AGCM3.2 with 20-km grid. *J. Meteor. Soc. Japan* **2012**, *90A*, 233–258.
17. Endo, H.; Kitoh, A.; Ose, T.; Mizuta, R.; Kusunoki, S. Future changes and uncertainties in Asian precipitation simulated by multiphysics and multi-sea surface temperature ensemble experiments with high-resolution Meteorological Research Institute atmospheric general circulation models (MRI-AGCMs). *J. Geophys. Res.* **2012**, *117*, doi:10.1029/2012JD017874.
18. Kitoh, A.; Ose, T.; Kurihara, K.; Kusunoki, S.; Sugi, M. KAKUSHIN Team-3 Modeling Group. Projection of changes in future weather extremes using super-high-resolution global and regional atmospheric models in the KAKUSHIN program: Results of preliminary experiments. *Hydrol. Res. Lett.* **2009**, *3*, 49–53.
19. The Weather Research and Forecasting (WRF). Available online: http://wrf-model.org/ (accessed online 30 January 2014).
20. Piani, C.; Haerter, J.O.; Coppola, E. Statistical bias correction for daily precipitation in regional climate models over Europe. *Theor. Appl. Climatol*. **2010**, *99*, 187–192.
21. Taiwan Climate Change Projection & Information Platform (CCIP). Available online: http://tccip.ncdr.nat.gov.tw/NCDR/main/index.aspx (accessed online 30 January 2014).
22. Shih, D.S. Analysis of typhoon-induced rainfall patterns (in Chinese). Master's Thesis, National Central University, Jhongli, Taiwan, May 2001; p.141.
23. Bobee, B.; Ashkar, F. *The Gamma Family and Derived Distributions Applied in Hydrology*; Water Resources Publications: Fort Collins, CO, USA, 1991.
24. Griffis, V.W.; Stedinger, J.R. Log-pearson type 3 distribution and its application in flood frequency analysis. I: Distribution characteristics. *J. Hydrol. Eng*. **2007**, *12*, 482–491.
25. Chow, V.T.; Maidment, D.R.; Mays, L.W. *Applied Hydrology*; McGraw-Hill Publishing Company: New York, NY, USA, 1988; pp. 380–491.
26. Kite, G.W. *Frequency and Risk Analysis in Hydrology*; Water Resources Publications: Fort Collins, CO, USA, 1977.
27. Cheng, K.S.; Lin, G.F.; Yu, G.H.; Lee, K.T.; Wang, R.Y.; Hsu, M.H., Yu, P.S. *Hydrologic Design Application HandBook* (in Chinese); Water Resources Bureau Research Reports; National Taiwan University, Department of Biological Environmental Systems Engineering: Taipei, Taiwan, 2001.
28. Efron, B.; Tibshirani, R. *An Introduction to the Bootstrap*; Chapman & Hall/CRC: Boca Raton, FL, USA, 1993; p. 456.
29. Takasao, T.; Takara, K.; Shimizu, A. A basic study on frequency analysis of hydrologic data in the Lake Biwa basin, Annual of Disas (in Japanese). *Prev. Res. Inst. Kyoto Univ*. **1986**, *29*, 157–171.
30. Fukami, K.; Sugiura, Y.; Magome, J.; Kawakami, T. *Integrated Flood Analysis System (IFAS Ver. 1.2), User's Manual*; Japan PWRI-Technical Note No.4148; Publisher: Tshukuba, Japan, 2009; p. 223.
31. Sugiura, T.; Fukami, K.; Fujiwara, N.; Hamaguchi, K.; Nakamura, S.; Hironaka, S.; Nakamura, K.; Wada, T.; Ishikawa, M.; Shimizu, T.; *et al*. Development of Integrated Flood Analysis System (IFAS) and its applications. In Proceedings of the Conference on Hydroinfomatics, Concepción, Chile, 12-16 January 2009; doi:10.1061/40976(316)279.

32. Aziz, A.; Tanaka, S. Regional parameterization and applicability of Integrated Flood Analysis System (IFAS) for flood forecasting of upper-middle Indus River. *Pak. J. Meteorol*. **2011**, *8*, 21–38.
33. Yoshino, F.; Yoshitani, J.; Sugiura, M. A conceptual distributed model for large-scale mountainous basins. In *Hydrology of Mountainous Regions. I—Hydrological Measurements*; *the Water Cycle*; Lang, H., Musy, A., Eds.; IAHS Publisher: Lausanne, Switzerland, 1990; pp. 685–692.
34. Hydrological Data and Maps Based on SHuttle Elevation Derivatives at Multiple Scales (HydroSHEDS). Available online: http://hydrosheds.cr.usgs.gov/index.php (accessed on 31 October 2013).
35. International Steering Committee for Global Mapping (ISCGM). Available online: http://iscgm.org/cgi-bin/fswiki/wiki.cgi (accessed on 31 October 2013).
36. UNEP. GNV25 Soil water holding capacity. Available online: http://www.grid.unep.ch/data/data.php (accessed on 31 October 2013).
37. Thiessen, A.H. Precipitation averages for large areas. *Mon. Weather Rev*. **1911**, *39*, 1082–1084.
38. Kimura, N.; Chiang, S.; Wei, H.P.; Su, Y.F.; Chu, J.L.; Cheng, C.T.; Liou, J.J.; Chen, Y.M.; Lin, L.Y. Hydrological flood simulation to Tsengwen reservoir watershed under global climate change with 20 km mesh Meteorological Research Institute atmospheric general circulation model (MRI-AGCM). *Terr. Atmos. Ocean. Sci*. **2013**, submitted for publication.
39. Nash, J.E.; Sutcliffe, J.V. River flow forecasting through conceptual models: Part I—A discussion of principles. *J. Hydrol*. **1970**, *10*, 282–290.
40. Yeh, C.L.; Yang, S.H.; Wei, S.T.; Hsieh, T.C. *Review and Application of the River Warning Level and the Regional Drainage Alert by Rainfall* (in Chinese); Water Resources Agency, Republic of China Ministry of Economic Affairs: Taipei, Taiwan, 2010.
41. Liu, K.F.; Wu, Y.H.; Chen, Y.C.; Chiu, Y.J.; Shih, S.S. Large-scale simulation of watershed mass transport: A case study of Tsengwen reservoir watershed, southwest Taiwan. *Nat. Hazards* **2013**, *67*, 855–867.

© 2014 by the authors; licensee MDPI, Basel, Switzerland. This article is an open access article distributed under the terms and conditions of the Creative Commons Attribution license (http://creativecommons.org/licenses/by/3.0/).